In reference to AMT-2021-406 "Measurement of vertical atmospheric density profile from the X-ray Earth occultation of the Crab Nebula with *Insight*-HXMT":

The authors are very grateful to the referees for their valuable comments and suggestions. Our responses to these comments are as follows.

Comments from reviewers:

Reviewer #2:

General comments:

1. **This paper presents a new measurement of the atmospheric density, based on the atmospheric occultation of X-ray emission from the Crab Nebula observed with *Insight*-HXMT. The authors analyzed a single egress event occurred on 2018-09-30T15:38:36. They showed that the density in altitude range of 105-200 km, 95-125 km, and 85-110 km are 88.8% (109.7%), 81.0% (92.3%), and 87.7% (101.4%) of the density prediction by NRLMSISE-00 (NRLMSIS 2.0), respectively. The density is qualitatively consistent with the previous results with RXTE. This study clearly demonstrates that *Insight*-HXMT can provide an approach for the study of the occultation sounding of the upper atmosphere.**

Reply: Thanks to the reviewer's comprehensive summary of the work and inspiring comments. The manuscript has been revised carefully based on the received comments. For details, please see the following responses.

Specific comments:

1. **I suggest the authors to estimate the uncertainty on the tangent point altitude. Two main sources of altitude errors are satellite position and pointing direction. Currently, the authors assume that these two parameters are perfectly known. However, it would be better to quantitatively give their errors and estimate how the errors affect the tangent altitude.**

Reply: Thank you very much for your valuable comments. We first analyzed the tangent point altitude errors from the satellite position. Monte Carlo simulation combined with satellite position measurement errors was used to give the uncertainties of the tangent point altitudes. The total position deviation of *Insight*-HXMT is 100 m under 3σ (3 standard deviation). We conducted 100 independent Gaussian sampling in the x and y directions of the satellite with $\mu = 0$ and $\sigma_x = \sigma/3$ ($\sigma_y = \sigma/3$). The standard deviation of satellite in the z direction is obtained by Eq. (1). The Gaussian noises were added to each direction of the satellite positions. Based on the satellite positions after adding noises, we calculated the tangent point altitudes. We analyzed the altitude errors caused by satellite position measurement errors and also estimate the density fitting errors caused by

uncertainties of the tangent point altitudes. The noise in one sample from one hundred independent Gaussian samples in the three directions is shown in FIG. 1 in this Response, where each sample in each direction has 552 points corresponding to 552 tangent point altitudes. Adding the corresponding noises in each direction of the satellite positions, we obtain the simulated positions of the satellite, as shown in FIG. 2 in this Response, which are the foundation for calculating the tangent point altitudes.

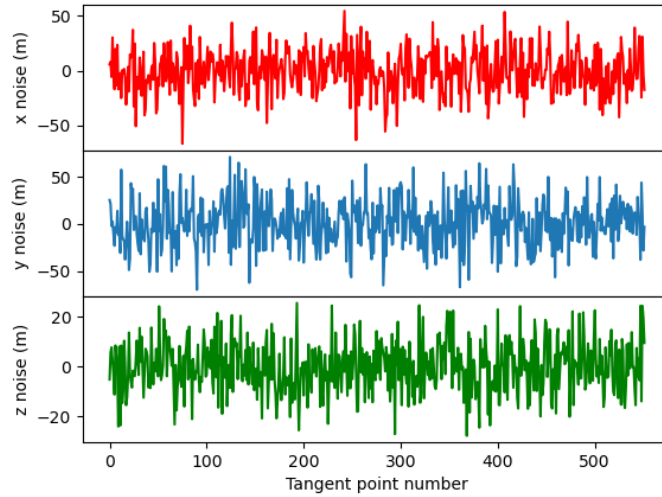$$\sigma_x^2 + \sigma_y^2 + \sigma_z^2 = \sigma^2 \tag{1}$$

FIG. 1 in this Response: The noise in one sample from one hundred independent Gaussian samples in the three directions.
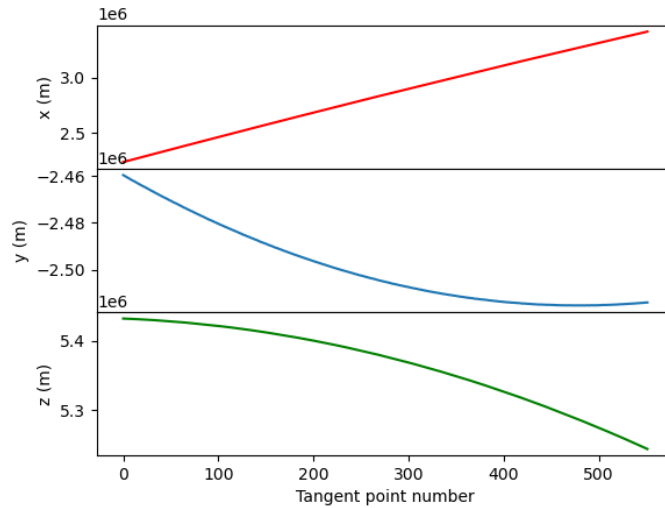

FIG. 2 in this Response: The simulated satellite positions after adding Gaussian noise to each direction of the satellite position.

The corresponding tangent point altitudes were obtained by analyzing the satellite position after adding noise, as shown in FIG. 3 in this Response. It was found that the error of the satellite's position resulted in a maximum deviation of about 40 m for the test tangent point altitude and the real altitude in the original manuscript, as shown the lower panel in FIG 3. in this Response.
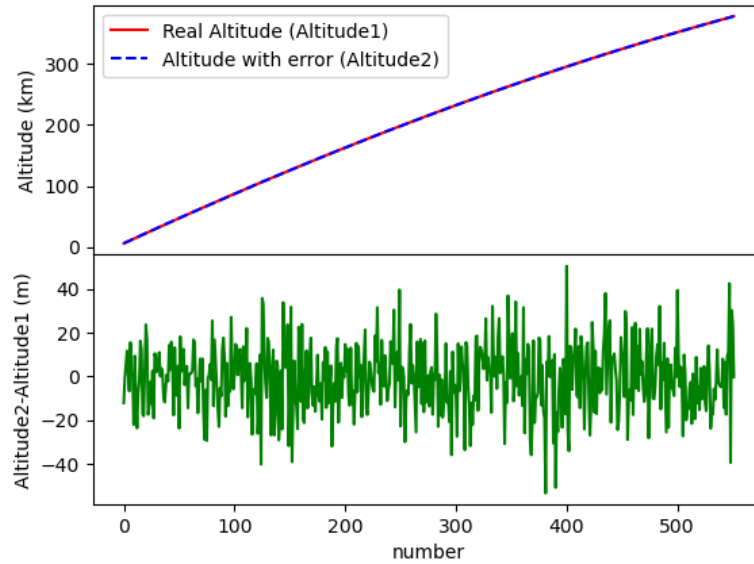

FIG. 3 in this Response: The comparison between the simulated tangent altitude and the real altitudes (upper panel).The difference between the simulated tangent altitude and the real altitudes (lower panel).

The atmospheric density was fitted based on the simulated altitudes with error, and the value of correction factor γ was obtained. Since we had taken one hundred independent samples of Gaussian noise for the satellite position, we can get one hundred γ values.

Table 1 in this Response. The fitted one hundred γ values based on one hundred simulated tangent altitudes with error.

Number	1	2	3	4	5	6	7	8	9	10
γ	0.886361	0.886189	0.889484	0.887557	0.887338	0.887903	0.888294	0.885130	0.887975	0.888256
Number	11	12	13	14	15	16	17	18	19	20
γ	0.887792	0.886524	0.886981	0.888782	0.886298	0.886432	0.885342	0.887291	0.885377	0.886704

Number	21	22	23	24	25	26	27	28	29	30
γ	0.887477	0.887847	0.889383	0.885718	0.888707	0.886319	0.886040	0.889365	0.888271	0.890716

Number	31	32	33	34	35	36	37	38	39	40
γ	0.886064	0.889049	0.887571	0.887625	0.887682	0.888805	0.887769	0.886466	0.887387	0.886382

Number	41	42	43	44	45	46	47	48	49	50
γ	0.888116	0.887688	0.887036	0.885247	0.888977	0.886960	0.889081	0.890935	0.887302	0.888472

Number	51	52	53	54	55	56	57	58	59	60
γ	0.885955	0.888675	0.886698	0.887132	0.886116	0.888758	0.885437	0.886343	0.889651	0.884448

Number	61	62	63	64	65	66	67	68	69	70
γ	0.885307	0.887394	0.888518	0.890139	0.887470	0.886591	0.887623	0.887347	0.888659	0.887169

Number	71	72	73	74	75	76	77	78	79	80
γ	0.887695	0.888246	0.885270	0.888409	0.887954	0.889285	0.886362	0.887950	0.887805	0.888645

Number	81	82	83	84	85	86	87	88	89	90
γ	0.889220	0.887716	0.885728	0.886952	0.885945	0.886264	0.886824	0.887072	0.887083	0.888430

Number	91	92	93	94	95	96	97	98	99	100
γ	0.888386	0.887020	0.888858	0.888251	0.888904	0.885684	0.886363	0.886484	0.887122	0.886926

To show more clearly the relationship between the one hundred γ values and the γ values based on real altitude, we plotted the distribution of the one hundred sample results, as shown in FIG.4 in this Response. It is found that the error of satellite position has little

influence on the final retrieved results (the retrieved density results are all within the real density value $\pm 1\sigma$).
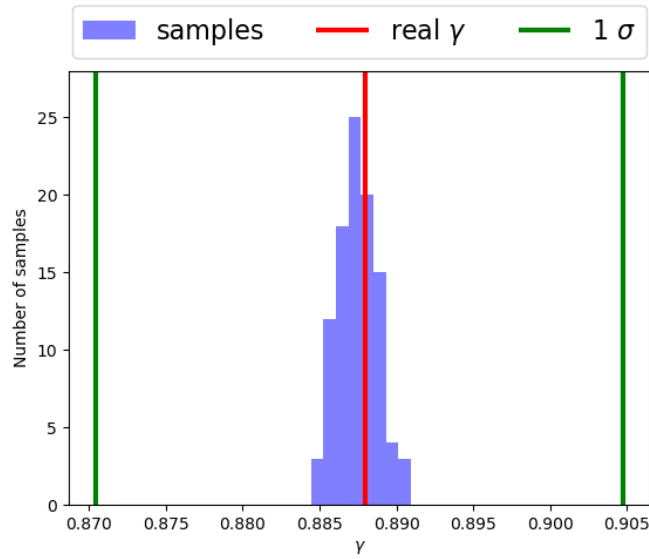

FIG. 4 in this Response: The values corresponding to the solid red line represent the retrieved results of γ by fitting the light curve in the energy range of 1.0-2.5 keV, the solid green line represents the real value ± 1 σ. The shaded blue area shows the distribution of one hundred γ sample values. It is found that the error of satellite position has little influence on the final retrieved results
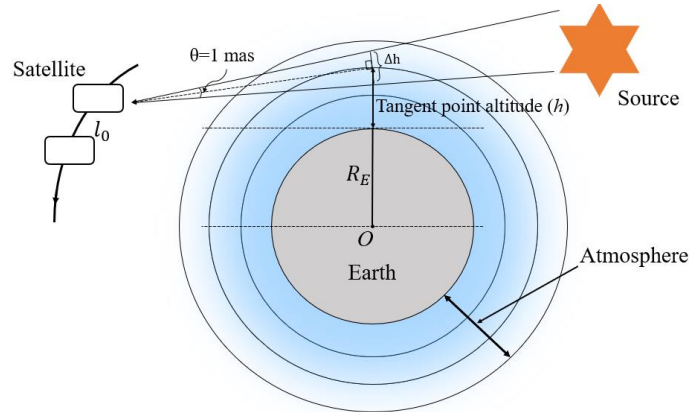

FIG. 5 in this Response: Observe geometry. The tangent height deviation ($\triangle$ h) caused by the position error of the source (1 mas).

Then we analyzed the tangent point altitudes error caused by the source position error. If the position of the source is offset by 1 milliarcsecond, then the tangent height deviation ($\triangle$ h) can be calculated. Through calculation, it is found that the tangent point altitude error caused by the position error of the source is on the order of centimetres or

millimetres, so the tangent point altitude error caused by the source position error can be ignored, because the tangent point altitude error is too small. As shown in FIG. 6 in this Response.
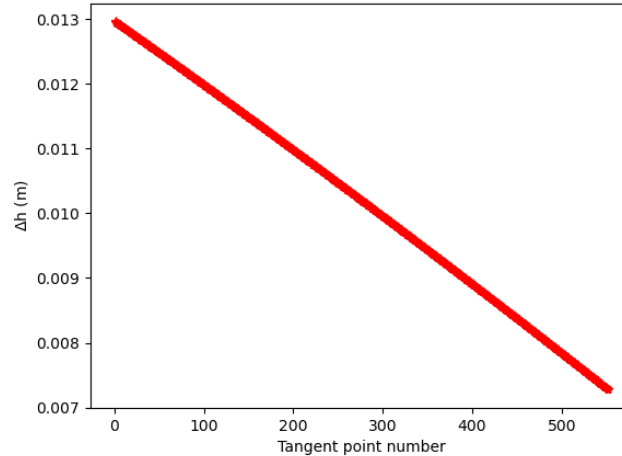

FIG. 6   in this Response: Tangent height error (Δ h) due to source error (1 milliarc second).

There are two main factors that can affect the tangent point altitudes according to our calculation process of the tangent point altitudes, namely, the position of the satellite and the position of the observation source. Through the above calculation, we have obtained the tangent point altitude error caused by the satellite position error and the tangent point error caused by the source position error. It is found that the tangent point altitude error caused by satellite position error and source position error can be ignored because it has little influence on the final retrieved density.

In addition, you mentioned the influence of satellite pointing direction on the tangent point altitudes error. The precision of pointing of *Insight*-HXMT: ≤0.1 degree (3σ), the precision of measurement: ≤0.01 degree (3σ), and the stability of pointing: ≤ 0.005 degree/s (3σ). We think that the pointing direction will not affect the calculation of the tangent altitudes. *Insight*-HXMT is a collimated satellite, the field of view of LE detectors is 1.6 °*6 °. We correct the response of the collimator effect in the response matrix file when the incident direction of the photon is not perpendicular to the detector plane. The satellite may have jitter when it points to a required source, and this will lead to the change of the source direction to the detector plane and also the detected rate of the photons. This effect is considered in the response matrix file.

2. Table 5 and Figure 13: It may be interesting to add the light curve in 1.0-2.5 keV, because the lower-energy band (i.e., higher altitude) seems more sensitive to the solar activity. Also, it would be better to bin the data (rather than sub-sampling as the authors did in the current paper) to improve the photon statistics.

Reply: Thank you very much for your valuable suggestions. According to your suggestion, we added the lightcurves in the energy range of 1.0–2.5 keV, because the lower energy range corresponds to a higher tangent point altitude during occultation, and the higher altitude is more sensitive to solar activity, as shown in panel (a) in FIG. 7 in this Response. In addition, we also added the lightcurve in the energy range of 6.0–10.0 keV to compare the influence of solar and geomagnetic activities on different altitudes, as shown in panel (c) in FIG. 6 in this Response. The Akaike information criterion (AIC) and the Bayesian information criterion (BIC) are calculated for these model comparisons and the results are listed in Table 2 in this Response. Goodness of fit between the observed lightcurve and the model lightcurves under the different solar activities and geomagnetic activities is also evaluated by $\chi^2/$dof and p-value in Table 1 in this Response. It is found that the solar activity and the geomagnetic activity have great influence on the shape of model lightcurves. In addition, with the increase of altitude, solar and geomagnetic activities have a greater impact on the model lightcurves.
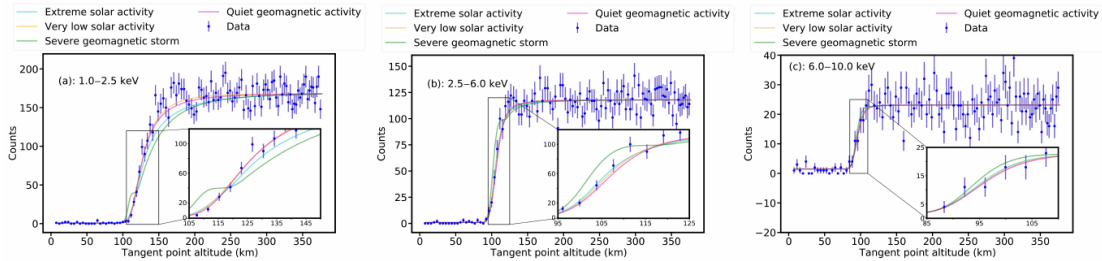

FIG. 7 in this Response: Comparison of the observed data and forward model lightcurves under extreme solar activity, very low solar activity, severe geomagnetic storm, quiet geomagnetic activity. For clarity, the data points are displayed by taking one point every five points from the initial data points. The energy range of the lightcurves in panel (a), (b) and (c) is 1–2.5 keV, 2.5–6.0 keV and 6.0–10.0 keV, respectively. Furthermore, local magnification of the lightcurves in the altitude range of 105–150 km, 95–125 km and 85–110 km is carried out to show the influence of solar and geomagnetic activities on the shape of the model lightcurves in panel (a), (b) and (c), respectively.

Table 2 in this Response. The calculated values of AIC, BIC, χ^2/dof and p-value.

Energy	Model	AIC	BIC	χ^2/dof	p-value
1.0–2.5 keV	Extreme solar activity	347.7317	358.3515	3.0768	0.0
	Very low solar activity	153.6371	164.2570	1.2890	0.0177
	Severe geomagnetic storm	704.2318	714.8516	6.2610	0.0
	Quiet geomagnetic activity	181.7213	192.3412	1.5636	$7.3075*10^{-5}$
2.5–6.0 keV	Extreme solar activity	50.3180	60.9379	1.2735	0.1177
	Very low solar activity	53.2962	63.9160	1.3831	0.0562
	Severe geomagnetic storm	152.6819	163.3017	3.4441	$2.1303*10^{-12}$
	Quiet geomagnetic activity	71.0399	81.6597	1.9109	0.0005
6.0–10.0 keV	Extreme solar activity	40.4108	51.0307	1.1069	0.3118
	Very low solar activity	40.9783	51.5981	1.1646	0.2422
	Severe geomagnetic storm	42.8781	53.4980	1.0945	0.3282
	Quiet geomagnetic activity	41.4147	52.0346	1.1842	0.2211

The final selection of photon statistics is mainly related to two factors, one is the selection of time bin (binsize) during data reduction (similar to exposure time), the other is the bin of energy channel.

The choice of binsize mainly affects the spatial resolution of the tangent point altitudes (δ h), that is, the distance between adjacent tangent point altitudes, as shown in Table 3 in this Response. The selection criteria of spatial resolution of tangent point altitudes is that the larger the better, that is, the smaller the distance between adjacent tangent points is, the better, that is, the smaller the binsize is. However, pursuing a smaller binsize can lead to another bad situation, namely, poor photon statistics. Therefore, we need to seek a balance between time bin and photon statistics. The selection criteria is that time bin should not be too large (if it is too large, the spatial resolution of the tangent point altitudes is too small), and photon statistics should not be too small. FIG. 8 in this Response shows the maximum distance, minimum distance and mean distance between adjacent tangent points corresponding to different binsizes. It is found that the distance between adjacent tangent points increases with the increase of binsize.

Table 3 in this Response: The corresponding relationship between time bin (binsize) during data reduction and the spatial resolution of the tangent point altitudes.

binsize (s)	0.1	0.2	0.3	0.4	0.5
Max δh (m)	207.8282	415.5873	623.2774	836.8984	1.0385e+03
Min δh (m)	123.4646	247.0097	370.3937	494.3417	618.1286
Mean δh (m)	166.6872	333.3754	499.9465	673.7546	833.4456

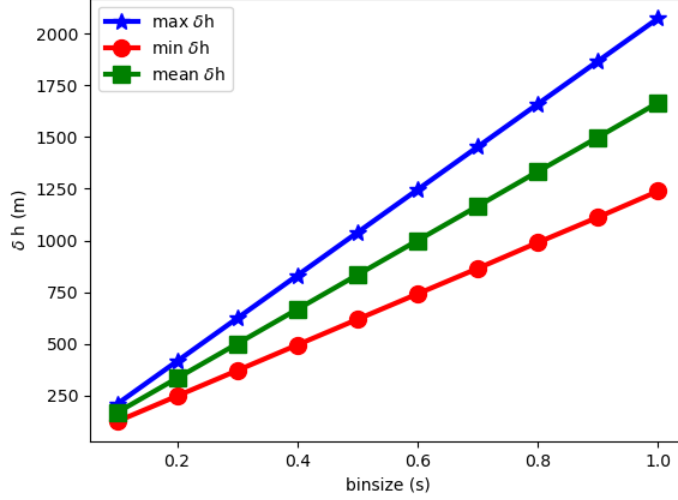| binsize (s)	0.6	0.7	0.8	0.9	1.0
Max δh (m)	1.2459e+03	1.4533e+03	1.6607e+03	1.8680e+03	2.0752e+03
Min δh (m)	741.5126	864.5340	989.9727	1.1123e+03	1.2383e+03
Mean δh (m)	999.9016	1.1661e+03	1.3335e+03	1.4993e+03	1.6669e+03

FIG. 8 in this Response: Maximum distance, minimum distance, and average distance between adjacent tangent points at different binsizes.

In addition, we calculated the average intensity (mean photon counts) of the unattenuated part of the lightcurves in the energy range of 1.0-2.5 keV, 2.5-6.0 keV and 6.0-10.0 keV corresponding to different binsizes, as shown in Table 4 in this Response. FIG. 9 in this Response shows the average photon counts of unattenuated part of the lightcurves in the energy range of 1.0-2.5 keV, 2.5-6.0 keV and 6.0-10.0 keV for different binsizes.

Table 4 in this Response: The corresponding relationship between time bin (binsize) during data reduction and the unattenuated mean intensity of lightcurves in the energy range of 1.0-2.5 keV, 2.5-6.0 keV and 6.0-10.0 keV.

binsize (s)	0.1	0.2	0.3	0.4	0.5
1.0-2.5 keV	40.4351	80.8621	121.0734	161.7500	202.1584
2.5-6.0 keV	28.1135	56.2196	84.1766	112.4565	140.5792
6.0-10.0 keV	5.6322	11.2686	16.8723	22.5217	28.1357

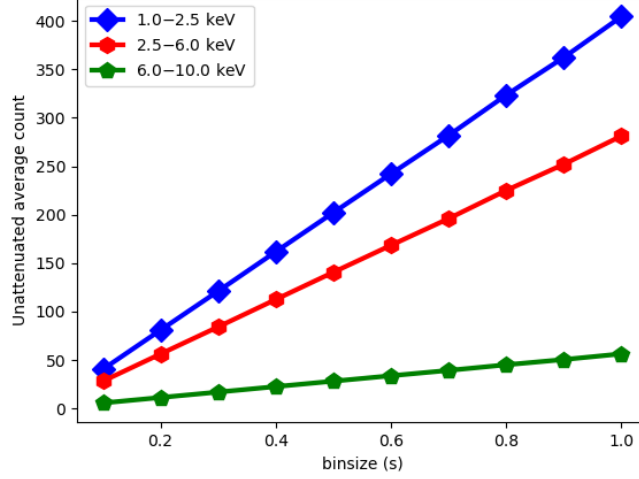| binsize (s)	0.6	0.7	0.8	0.9	1.0
1.0-2.5 keV	242.1784	281.7799	323.4964	362.3306	404.4595
2.5-6.0 keV	168.3946	195.9308	225.0432	252.0565	281.2252
6.0-10.0 keV	33.7297	39.2453	45.0360	50.4516	56.3333

FIG. 9 in this Response: Average intensity (mean photon counts) of the unattenuated part of the lightcurves in the energy range of 1.0-2.5 keV, 2.5-6.0 keV and 6.0-10.0 keV under different binsizes.

Through the above discussion, we finally choose binsize=0.4s, because the spatial resolution of the tangent point altitudes corresponding to this value is high enough (the average distance between two adjacent tangent points is about 673 meters), and the lightcurves in the energy range of 1.0-2.5 keV, 2.5-6.0 keV and 6.0-10.0 keV corresponding to this value has relatively high photon statistics. In summary, the signal-to-noise ratio of X-ray photon counting is greater than 4 and the resolution of the tangent point altitude is high enough (less than 1 km)，so binsize=0.4 s is finally selected.

In addition, photon counting statistics was also considered in the our fitting. Taking into account the the Poisson nature of our data, the Poisson statistics were used instead of Gaussian statistics in the Markov Chain Monte Carlo sampling. The X-ray counts is different from the detection for traditional ultraviolet, visible and infrared wavelengths. Poisson statistics were used as the likelihood function and C statistics as the logarithmic likelihood function, because C statistics as the logarithmic likelihood function would lead to smaller errors compared with Chi-square statistics[1].

The specific form of Poisson statistics is as follows:

$$\mathcal{L} = \prod_i \frac{M_i^{D_i}}{D_i!} \exp(-M_i) \qquad (2)$$

The specific form of C statistics is as follows:

$$C = 2 \sum_i [M_i - D_i + D_i(\log D_i - \log M_i)] \qquad (3)$$

Reference:

[1] Nousek, J. A. and Shue, D. R., "Chi-squared and C Statistic Minimization for Low Count per Bin Data", The Astrophysical Journal, vol. 342, p. 1207, 1989. doi:10.1086/167676.